TDEM prospections for inland groundwater exploration in semiarid climate, Island of Fogo, Cape Verde

TDEM prospections for inland groundwater exploration in semiarid climate, Island of Fogo, Cape Verde.

Amato F. [1], Pace F. [2], Vergnano A.[2] and Comina C.[1]
[1]DST, Dipartimento di Scienze della Terra, Università degli studi di Torino, Torino (IT)
[2] DIATI, Dipartimento di Ingegneria dell'Ambiente, del Territorio e delle Infrastrutture, Politecnico di Torino, Torino (IT).

ABSTRACT
Groundwater resource assessment is fundamental for agriculture in arid or semiarid conditions, where precipitations are irregular and scarce. In volcanic islands, groundwater resources are often located at significative depths, thus hindering direct exploration. The application of geophysical techniques is therefore necessary for a preliminary evaluation of water availability and to identify potential drilling points. In this study, Time Domain Electromagnetic Method (TDEM) soundings were used for groundwater prospection in the surroundings of a vineyard on the island of Fogo, Cape Verde. A pseudo-2D profile of ten sounding points was located within the vineyard, and other localized prospections were performed close to known boreholes, for attempting correlations of TDEM evidence with water depth and stratigraphy. The data acquired were interpreted by means of three inversion algorithms to obtain an uncertainty evaluation of the results. Particularly, the particle-swarm-optimization algorithm, the linearized 1D inversion and the spatially constrained inversion were applied. These methods provided a set of equivalent solutions of the TDEM inverse problem to be evaluated and compared. The inverted models are highly consistent and show little mismatch at greater depths. The main outcome regarding the resistivity distribution in the vineyard subsurface is the evidence of a nearly 150 m-thick conductive region (1-10 Ωm). Information from existent water wells enhanced the hydrogeological interpretation of the profiles and the detection of potential water-saturated formations.

Keywords: Time-domain Electromagnetics (TDEM), spatially constrained inversion (SCI), particle swarm optimization (PSO), groundwater resources, Cape Verde, volcanic islands.
Corresponding author: Cesare Comina, cesare.comina@unito.it

1. INTRODUCTION

Groundwater resource assessment is fundamental in volcanic islands under arid or semiarid conditions with irregular and scarce precipitations. Rainfall is conditioned by altitude, morphology and orientation to the prevailing winds, and groundwater resources depend on the thickness and variability of the potential water-bearing formations. Besides, dew condensation and fog interception can be an important source of water for some islands in arid climatic zones (Falkland and Custodio, 1991).

Hydrogeological models in volcanic island context (e.g. Heilweil et al., 2005) often consider a subsurface composed of stratified basaltic lava flows with intervals of pyroclastic rocks, breccias and mafic dykes. Basalts and pyroclastic rocks have very variable hydraulic conductivity (Freeze et al., 1979) depending on their fracturing conditions (Gingerich and Voss, 2005) and can host exploitable groundwater resources. On the contrary, dykes and low hydraulic conductivity rocks (i.e., clayey weathered volcanic formations, paleosoils and even the same pyroclastic rocks) usually act as impermeable barriers. In a similar geological context with respect to the present paper, i.e. Santiago island in Cape Verde, Gonçalves et al., 2017 reported the presence of basic breeches and pyroclasts with great extent and uniformity showing a high rate of compactness and low permeability and formations composed by pyroclastic material cones and associated leakage with a high degree of permeability and porosity. Because of this, and of the complex geometries in the subsurface of volcanic areas, perched aquifers can often be found.

The main water resource is usually located at great depth just above the seawater level (Falkland and Custodio, 1991), due to difficult climatic conditions, such as irregular rainfall, and adverse geological conditions, such as extremely permeable rocks (of volcanic origin or karstified limestone). Near the coastline, due to their difference in density, thin freshwater lenses float above seawater and these are often the most exploited water resources. This fresh/seawater balance is however very weak and can be compromised: when freshwater is excessively pumped, a retrieval of seawater can be generated, causing saline intrusion into the inland. Moreover, water delivery inland from the coastline can be complicated, due to the necessity to build large, expensive pipelines. Inland agricultural developments can therefore suffer from water shortages due to the absence of continuous and reliable water resource availability.

Far from the coastline of the island of Fogo, Cape Verde, the studied vineyard (Figure 1a-c) is indeed facing with water scarcity. The vineyard (Figure 1d) is located at an altitude between 650 and 900 meters a.s.l. and has an extension of 25 hectares. It was planted within a cooperation project by the AMSES (Associazione Missionaria Solidarietà e Sviluppo) Italian non-profit organisation of social utility in 2009. Given the considerable scarcity of water at this elevation, a fixed drop irrigation

system was built for watering the grape plants. The water supply functions through the connection to the nearest tank of the public aqueduct, which required the drafting of a 6-kilometer pipeline and the positioning of a storage tank in the vineyard. At the beginning of its activity, the vineyard had a satisfactory production. Nevertheless, in the last three years, the severe water scarcity that has affected the island of Fogo has strongly compromised the water supply to the vineyard. Therefore, the aim of Amses Onlus is to drill a water well in the proximity of the vineyard to increase water availability. However, within this setting, drilling a new water well is not an easy task due to significant logistical limitations and technical issues typical of a developing country (e.g. availability of proper drilling apparatuses). Therefore, the application of rapid and cost-effective geophysical techniques is of pivotal importance for a preliminary evaluation of water availability and to identify specific and potentially successful drilling points.

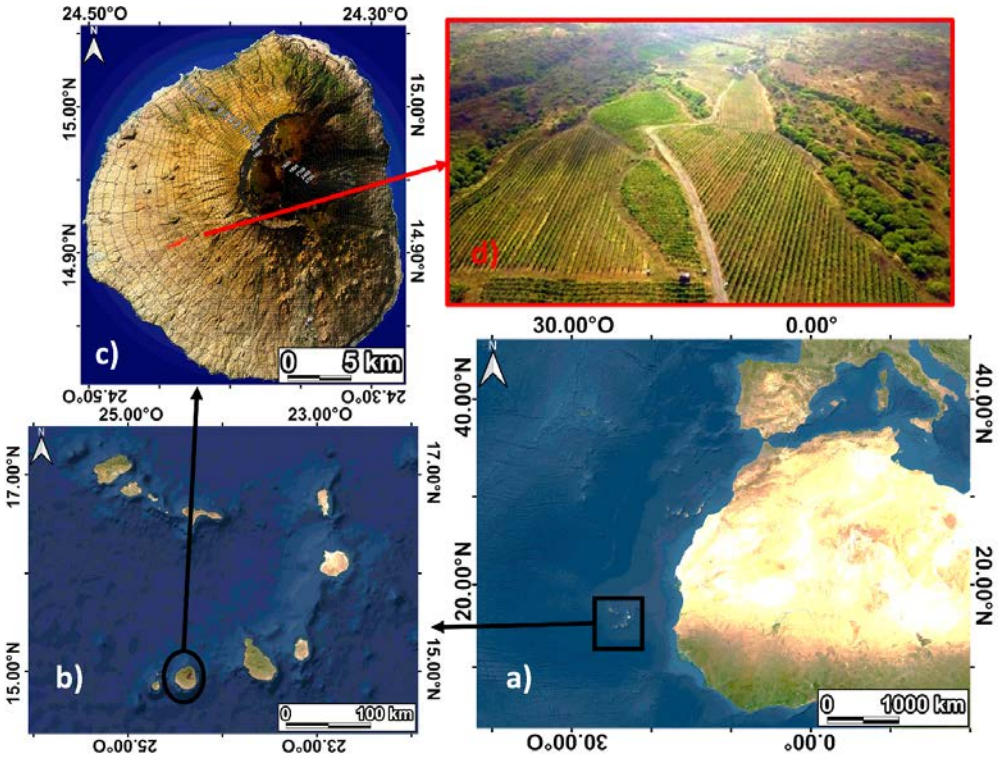

Figure 1 – Geographical location of the vineyard studied: a) and b) geographical location of the Cape Verde archipelago, c) detail of Fogo Island with evidence of vineyard location (red box) and d) detail on the vineyard investigated.

Among the various available geophysical methods, the Time Domain Electromagnetic Method (TDEM) investigates underground resistivity distribution at greater depths and is of easier application than other geoelectrical methods usually adopted for water resource assessment. TDEM soundings have been widely applied to near-surface geology, mineral prospecting, hydrogeological and environmental investigations (e.g. Celico, 1988; Nabighian, 1991) and have already been successfully applied in volcanic contexts (e.g. Auken et al., 2009; Ruiz-Aguilar et al., 2010; Trota et al., 2019), in

the Cape Verde archipelago (e.g Gonçalves et al., 2017) and in the island of Fogo. Within Fogo, TDEM was applied by Martínez-Moreno et al. (2016) on a wide survey grid, evidencing the presence of a low-resistivity layer potentially correlated to a deep water table on the west side of the island. Moreover, Descloitres et al. (2000) highlighted the presence of a layer with intermediate-resistivity attributed either to partially or totally water-saturated volcanic rocks or to clayey layers between fractured lava flows.

The objective of the present work is to image the subsurface resistivity distribution of the vineyard by means of TDEM soundings. A pseudo-2D profile of ten sounding points was located within the vineyard, while other localized prospections were executed close to known boreholes, for attempting correlations of TDEM evidences with water depth and stratigraphy. The data acquired were interpreted by the use of multiple inversion algorithms to obtain an uncertainty estimate on the results. The final goal is then the hydrogeological interpretation of the resistivity profiles for groundwater resource location.

2. GEOLOGICAL AND HYDROGEOLOGICAL SETTING

The island of Fogo is situated southwest of the Cape Verde archipelago, which is located about 700 km west of Senegal (Figure 1a). Fogo is part of the so-called Sotavento islands, according to its position with respect to the dominant wind (trade winds), which blows from the North-East (Figure 1b). Fogo is the fourth largest island of the archipelago, has a circular shape with an area of 476 km^2 and an average width of about 25 km (Figure 1c). It has an asymmetrical conical shape due to the main volcanic building, the shield volcano Mt. Amarelo, which rises 2829 m above sea level and is mainly composed of basalts and minor pyroclastic products. The average slope varies between 12° and 25° depending on the side (less inclined to the south-west side where the vineyard is located). In the highest portion stands a nearly vertical wall, about 1000 m high, semi-circular in shape, open to the east and extending for about 20 km. The morphology of this wall, called Bordeira, is the consequence of the collapse of the caldera which truncated the original shape of the island (Day et al., 1999).

In Fogo, as in many other volcanic islands, the main factors that influence the presence of groundwater are the irregularity of the precipitation and the high slopes hindering infiltration. The recharge of the aquifer on the island is only minimally affected by the contribution of precipitation compared to that of high-altitude fog, which is formed due to the condensation of the clouds that occurs for the cooling of the trade winds. This phenomenon is relevant on the east side of the island, due to the presence of the Bordeira, but strongly reduced on the west side, where the vineyard is

located. According to Barbosa (2008), part of the water supplied by the little rainfall and fog ends up in the sea due to the runoff, while the remaining aliquot infiltrates into the ground.

The water accumulates at high depths due to the high permeability of the rocks, mainly fractured basalts and pyroclastic rocks (Mitchell-Thomé, 1972), that is comparable to the diaclases in the limestones (Machado and De Assunção, 1965). The infiltration stops only at the compact tufaceous levels that act as an impervious basement of the aquifer. A priori knowledge of the hydrogeological setting and groundwater depth could be important for the correct planning of the TDEM surveys.

Nevertheless, hydrogeological knowledge of Fogo island is limited due to the small number of wells, mainly located along the coastline (black-bounded circles in Figure 2a), where continuous monitoring of the piezometric level is missing but isolated information is available from a survey campaign of 2005 (Heilweil et al., 2005).

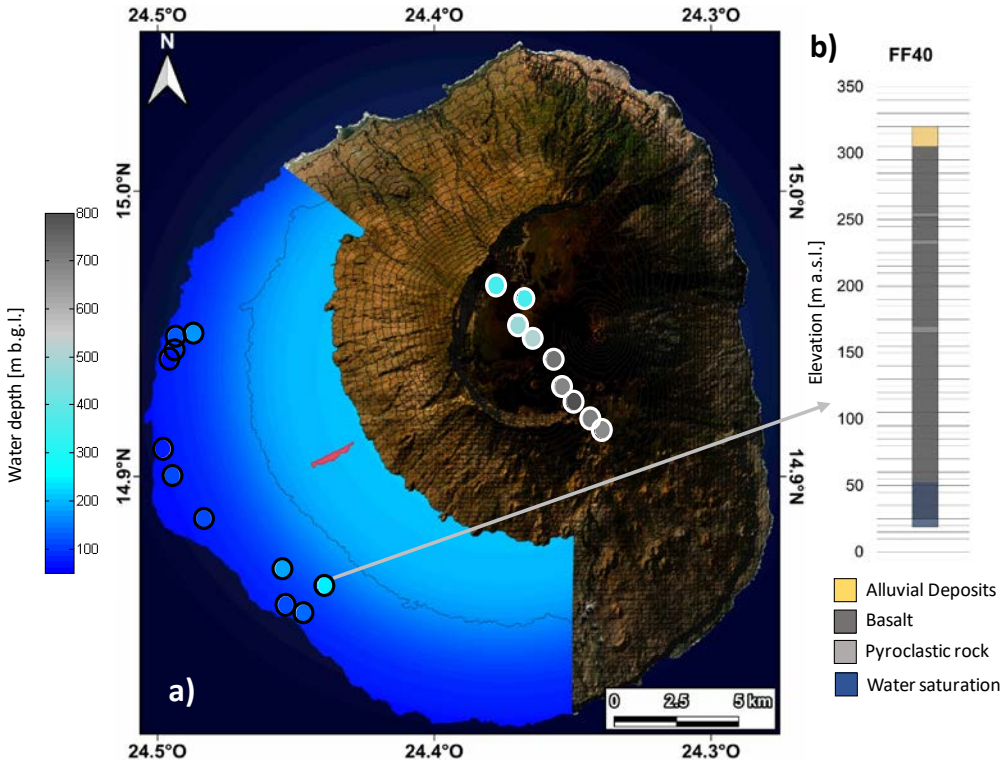

Figure 2 – Available hydrogeological information in Fogo Island: a) water depth below ground level from boreholes along the coastline (black-bounded circles), estimated water depth from the magnetotelluric profile of Martínez-Moreno et al. (2018) crossing the caldera (white-bounded circles) and from the TDEM surveys of Martínez-Moreno et al. (2016) (colored surface on the southwest flank), b) available stratigraphic log. The location of the studied vineyard is marked in red.

For this reason, it is very hard to define the average water table depth in the innermost portions of the island. Stratigraphic information obtained during the construction of the wells is also difficult to find. On the west side of the island, a number of boreholes were drilled in the past, but the only available

stratigraphic information (Agua Brava, personal communication) comes from a single water well (FF40) (Figure 2b). From this stratigraphic log, a thick and relatively uniform basalt formation is evidenced, with the localized presence of thin (around 5 m) pyroclastic layers, covered by 15 m of alluvial deposits. A similar geological setting is also reported in few other stratigraphies coming from the north side of the island, although the layers' alternation and thickness are different. It is worth noting the water-table depth of around 270 m b.g.l. for this well. This reflects in the high altitude of the water table with respect to the sea level (i.e. 50 m a.s.l.), not coherent with the Ghyben-Herzberg relation for stagnant seawater (Bear et al., 2010). A similar condition was detected in Santiago island by Gonçalves et al. (2017) observing that the Ghyben-Herzberg relation does not apply for inland portions of the island due to the extension of a conductive zone toward the land that cannot be explained with the seawater intrusion. The presence of clay lenses and perched aquifers is therefore most probable in this geological setting. Clay lenses were indeed detected in several locations near the sea level in Santiago island by Gonçalves et al. (2017). This kind of clay lenses near the sea level was also detected in multiple locations near the sea on the north coast of Fogo Island (Agua Brava, personal communication).

Due to the lack of direct information, Martínez-Moreno et al. (2016) carried out TDEM geophysical surveys with 26 sounding points on the southwest flank of the volcanic edifice. The interpretation of these soundings allowed obtaining a 3D model composed of 5 layers parallel to the topographic surface, evidencing the presence of a relevant decrease in resistivity (from one to two orders of magnitude) at variable depths. This drop was correlated with a possible water table. In fact, a widespread low resistivity region (below 10 Ωm) was detected below the high resistivity layers (500-1000 Ωm) of the shallow subsurface. This region was located at a depth of about 100-150 m b.g.l. for altitudes less than 500 m a.s.l. and of about 250 m b.g.l. between 500 and 1000 m a.s.l.; the results of this survey are reported in the colored surface in Figure 2a. Later, Martínez-Moreno et al. (2018) carried out two magnetotelluric profiles on the eastern side of the island to investigate the collapse structures of the caldera. Along with these profiles, conductive bodies in contact with resistive rocks were identified. The conductive bodies were interpreted as very permeable deposits formed by recent volcanic rocks (post-collapse sequence) saturated in water. The resistive bodies were interpreted as less permeable volcanic rocks belonging to the pre-collapse sequence. The magnetotelluric profile crossing the caldera indicated the approximate surface of the water table, which has a variable depth, ranging from about 370 m to about 800 m b.g.l. (white-bounded circles in Figure 2a). The outcomes of Martínez-Moreno et al. (2016, 2018) represent a benchmark for our investigation as they started geophysical prospection in Fogo Island. These results also give indications on the attended depth of

the groundwater resource from the coastline to the inland which is important information to compare with the evidence of our surveys.

3. METHODOLOGY

The TDEM method makes use of an active source that transmits a steady current (from 1 to 20 A) for some milliseconds through a loop of wire. The current has a slow rise-up to a steady value and then is interrupted by a rapid shut-off, in the order of microseconds. The shut-off transient induces eddy currents that generate a secondary magnetic field, which is proportional to their decay. The decay of the secondary magnetic field is measured by a receiver coil and is a function of the electrical resistivity distribution in the subsoil. The response at the receiver is usually acquired, for a number of time gates, during the transmitter off-time, because the primary field signal is weak or absent. The analysis of the transient decay of the secondary field with time allows the electrical resistivity to be estimated as a function of depth (Everett, 2013; Spichak, 2015).

The volume investigated by TDEM depends on the transmitted current and on the length of the side of the loop (usually between 20 and 200 m). The transmitter and receiver can be placed on the ground according to different configurations. The “coincident-loop” configuration makes use of transmitter and receiver loops having the same center.

The diffusion depth represents the depth at which the local electric field (or current) reaches its maximum value and is controlled by the transient time t. The relation of the diffusion depth is (Nabighian, 1991):

$$d(t) = \sqrt{\frac{2t}{\mu_0 \sigma}} \qquad (1)$$

where $d(t)$ is the diffusion depth, t is the time of the response measurement after the shut-off, μ_0 is the magnetic permeability in free space ($4\pi \cdot 10^{-7}$ Hm^{-1}) and σ is the electrical conductivity of the body. An approximate estimation of the sounding depth is usually indicated as 3 or 4 times the side of the transmitter loop (Spichak, 2015). Equation 1 suggests that the TDEM method is sensitive to conductive formations (like clay and seawater) in shallow-depth structures up to a theoretical depth of about 500 m (depending on the instrument and the sounding set up).

3.1 Survey setting and data acquisition

The survey was carried out in January 2020. TDEM data were acquired using the TEM-FAST 48 instrument by AEMR company. The acquisition configuration was a coincident loop of 100 x 100 m.

If the accessibility of the site was far from ideal, the loop was always displaced to enclose an area of around 10000 m^2 (Figure 3).

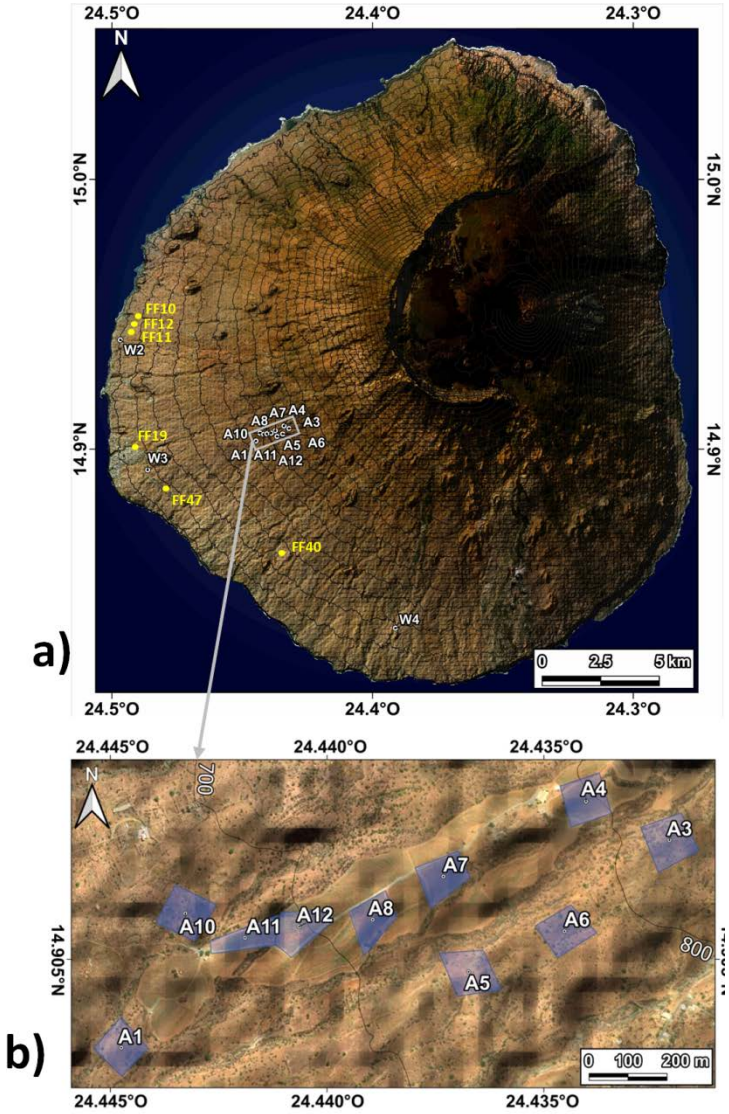

Figure 3 – TDEM surveys executed: a) all surveys executed, b) detail of the acquisition loops within the vineyard; available reference boreholes near to the survey locations are also reported in a) with yellow labels.

Ten TDEM soundings were acquired inside the vineyard, sites A1-A12 in Figure 3b and Table 1. The only a priori information about the supposed shape of the target in the subsoil is related to the Martínez-Moreno et al. (2016) survey, which depicts a water-table trend broadly following the topographic surface (Figure 2a). The sounding locations followed therefore the elongated SW-NE direction of the vineyard, nearly in the main slope direction of the terrain, in order to appraise the influence of the elevation on the resistivity distribution and, possibly, on the aquifer layers. Along this direction, the spacing between the soundings was kept as regular as possible, except for those cases of prohibitive areas (prickly plants, scarps), e.g., between sites A7 and A4 or A7 and A6. Sites A8, A11 and A12 present an irregular shape due to the partition of the vineyard parcels and to the

steep terrain configuration. The actual surface of those soundings was used to correct the signal amplitude by considering an equivalent circular-loop radius. Three more soundings were located outside the vineyard, sites W2-W4 in Figure 3a and Table 1.

Table 1 – TDEM surveys executed: geographical location of the loops. The coordinates are in WGS84 EPSG 4326 (registry for coordinate reference systems and coordinate transformations).

	Lat [°]	Long [°]	Elevation [m.a.s.l.]
A1	-24.445	14.903	633
A3	-24.432	14.908	815
A4	-24.434	14.909	798
A5	-24.437	14.905	737
A6	-24.435	14.906	770
A7	-24.437	14.907	752
A8	-24.439	14.906	720
A10	-24.443	14.906	674
A11	-24.442	14.906	680
A12	-24.441	14.906	697
W2	-24.497	14.941	88
W3	-24.486	14.892	176
W4	-24.391	14.833	295

The transmitted signal was 12 V and the effective injected current was 1.8 A. The turn-off time was 7-8 μs and the digital stacking of the signal was 10. The site acquisition was repeated to improve the response measurement from low to high time ranges, i.e., from 1 ms (first acquisition) to 16 ms (last acquisition). In fact, it is good practice to start with a maximum time range of 1 ms to avoid any distorted signals. Then, the time range can be increased up to 4 or 16 ms as long as the error bars are acceptable and the desired accuracy is ensured.

Few sites acquired within the vineyard presented a high level of noise, probably due to the high number of iron pickets buried in the ground and iron wires suspended in between for supporting the

rows of grapevines. For these sites, the relative TDEM signal curves (V/A) showed oscillatory values at early times (up to 0.5 ms). This oscillating response phenomenon is provoked by a "capacitive coupled" conductor (Danielsen et al., 2003; Sørensen et al., 2000) and happens when a nearby insulated cable is excited by the transmitter signal. These fluctuations usually take place at early times, and showed good repeatability. This effect was minimized by repeating the acquisition for increasing time ranges. For few sites, the final curve of the measured signal was obtained by extracting the less-distorted portion of the signal at different time ranges and then by merging these portions into a single a-posteriori curve. This procedure is shown in Fig. 4 for site A5.

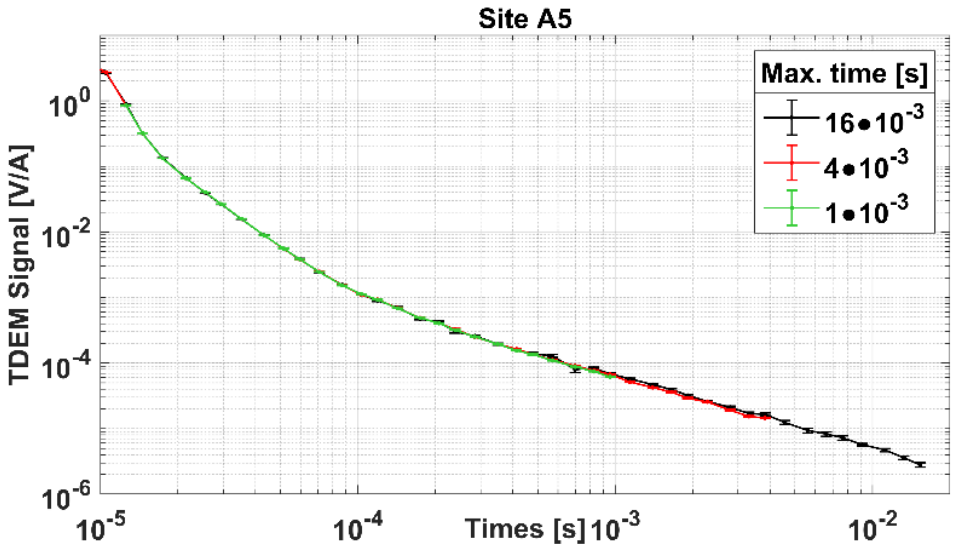

Figure 4 – Acquired signal with error bars for site A5 at increasing time ranges: 1 ms (green), 4 ms (red) and 16 ms (black). The final curve for the inversion was obtained after merging the final portions of each curve.

Moreover, comparing the cluster of acquisitions within the vineyard to those outside it, the former presents a constantly weaker response signal. According to Sørensen et al. (2000), this phenomenon happens when the interference is provoked by a nearby non-insulated metallic object, like a pipeline, which is "inductive coupled" to the ground. The several iron pickets, ditched into the ground and connected not only by suspended wires, but also by underground non-insulated wires, could have performed as non-insulated conductors. In this setting, the two phenomena, due to capacitive and inductive coupling, could have therefore acted at the same time.

3.2 Inversion

The interpretation of the observed TDEM data is accomplished by solving the inverse problem, which results in a one-dimensional model of the resistivity distribution in the subsurface of each sounding. Problem unknowns are the resistivities and thicknesses of the different layers. From a mathematical point of view, the inverse problem is ill-posed in nature with nonlinear and extremely sensitive

solutions. This means that many models can equally fit the data within a given tolerance threshold. Therefore, dealing with the inverse problem means solving a nonlinear, multi-parametric and ill-posed problem affected by the equivalence of solutions (Tarantola, 2005).

To ensure an uncertainty estimate on the obtained results and an evaluation of the equivalence issue, different inversion methods were applied to the acquired data. At first, a global-search method performing stochastic inverse modeling (Sen and Stoffa, 2013) was adopted to allow for a global initial estimate of the resistivity distribution. Global search methods have become of major interest in geophysics because they are theoretically able to find the global minimum of a function without being trapped in local minima (Sen and Stoffa, 2013). The final minimum misfit solution obtained with this approach, supposed to be near the global minimum, was then used as the starting point for the second inversion method adopted, based on a 1D local search approach. Local search approaches have the advantage of focusing the results on a single minimum parameterization profile thus allowing more precise considerations about geological information. The final inversion performed was a Spatially Constrained Inversion (SCI) of the profiles within the vineyard. This allowed a more consistent interpretation of all the profiles with the common reference geological setting.

All the inversions were implemented in Matlab routines using a forward modelling solver which considered a coincident-loop TDEM configuration for different transmitting and receiver loop sizes, as proposed by Ingeman-Nielsen and Baumgartner (2006).

3.2.1 Global PSO Inversion

Differently from traditional derivative-based inversion techniques, that perform a linearized inversion (i.e. local search methods), global-search methods sample the model space either randomly (e.g. Monte Carlo) or according to a specific strategy (e.g. adaptive behavior). The essential advantage of global search algorithms is that the final solution is independent of the initial guess of the starting model (Pace et al., 2019a).

A metaheuristic method called Particle Swarm Optimization (PSO), a nature-inspired population-based computational intelligence algorithm (Kennedy and Eberhart, 1995) was applied. In PSO a set of possible solutions is represented by a set of particles grouping in a swarm. The particles populate the search space of the problem solutions and change their position in order to minimize the objective function, which accounts for the data misfit and the model roughness (Pace et al., 2019b). Applications of the PSO for the inversion of electromagnetic geophysical data are provided in Godio and Santilano (2018) and Santilano et al. (2018), setting the field for the adopted PSO inversion scheme.

At the beginning of the optimization, the particles are initialized in the search space with a uniformly-distributed random position and null velocity. Then, the adaptive behavior begins: each iteration, each particle is stochastically accelerated, on one hand, toward its previous best position (i.e., where it minimized the objective function) and, on the other hand, toward the neighborhood best position (i.e., where any other particle minimized the objective function). These two basic approaches are referred to as exploration and exploitation, respectively. They compete in searching for the global optimum solution. While the exploration is associated with cognitive behavior, the exploitation is related to social behavior, that is, the convergence toward the leader. In order to balance exploration and exploitation of the search space, we applied an improved PSO variant called hierarchical PSO with time-variant acceleration coefficients (HPSO-TVAC) (Ratnaweera et al., 2004). This approach has demonstrated to enhance solution diversity at the beginning of the optimization, to avoid premature convergence to a local minimum and to ensure solution convergence and stability at the end of the optimization. Further details on the HPSO-TVAC application to geophysical data can be found in Pace et al. (2019a, 2019b).

To perform the optimization, the resistivity model was discretized into 19 layers, whose fixed thicknesses increased logarithmically with depth, according to the loss of resolving power. A couple of TDEM data required a coarser parametrization (sites W2 and W4). The diffusion depth (equation 1) associated with the soundings was between 360 and 500 m. The maximum depth of the model was chosen coherently to the maximum acquisition time of the signal. The number of particles, i.e. of the sampled solutions, was chosen proportionally to the number of unknowns, namely, 9 times the number of layers (Pace et al., 2019a). The boundary conditions of the search space represent the resistivity range of the possible solutions. They were set far larger than the apparent-resistivity range of each specific TDEM site and also by taking into account geological prior knowledge (Mota Gomes, 1994). Several PSO tests were performed to tune and define the proper lower and upper limits that ensured a wide coverage of the explored solutions. The PSO algorithm ran for a maximum of 500 iterations or stopped before if the objective function did not minimize for 100 consecutive iterations (alternative stopping criterion). Each run was launched 10 times (or ‘trials’) in order to test the solution variability coming from the initial random distributions.

3.2.2 Local 1D Inversion

A simple 1D inversion was later performed for each sounding curve. These inversions were performed with a damped least-squares inversion algorithm, considering both the layer resistivities and layer thicknesses as unknowns. With respect to the PSO parameterization, a reduced number of layers was adopted for these inversions. Different parameterizations (from 3 to 8 layers) were attempted for each site in order to reach the 1D minimum misfit solution for each site.

3.2.3 Local SCI Inversion

A further inversion approach was adopted for the soundings located within the vineyard, which had a denser spatial distribution. These last inversions were performed using a Spatially Constrained Inversion (SCI) algorithm in which all the TDEM soundings are inverted globally through a set of spatial constraints that tie each 1D local resistivity model to the neighbouring ones, to allow for an internally consistent representation of the investigated volume. In this way, a unique misfit function is used for all the soundings. This approach has already been applied to TDEM data (e.g. Viezzoli et al., 2008) and to several other types of geophysical data (e.g. Comina et al., 2012) and provides a pseudo-3D mapping of the subsurface. Further details on the specific SCI for TDEM data can be found in De Luca et al. (2018). For this inversion, a 6-layers parameterization was adopted with moderate constraints for the resistivities (500 Ωm variability) and layer thicknesses (50 m variability) among the models in order to allow for a uniform mapping of the subsurface without avoiding the potential presence of lateral variations. The strength of the constraints is described in the covariance matrices of the SCI formulation and is also weighted with the distance of the sounding points.

4. RESULTS

In Figure 5, example results of the acquired data and of the different inversions for the soundings within the vineyard are reported. Signal curves are reported to represent the experimental evidence of each sounding because all the inversion schemes adopted were based on the calculation of the predicted signal, not on the apparent resistivity curves as performed in other inversion schemes. It can be observed (Figure 5a, c and e) that all the performed inversions resulted in a satisfactory data misfit (on average below 3%) with the acquired TDEM signal, which showed also reduced standard deviation, as an indication of the quality of the acquired data.

All the inverted models (Figure 5b, d and f) are consistent in depicting a highly resistive (around 1000 Ωm) shallow portion till about 150 – 200 m depth followed by a low resistivity region (around 10 Ωm) till about 350 m depth. Below this low resistivity region, the imaged increase in resistivity should be considered with caution due to the limit of the TDEM investigation depth and underlying assumptions. The ambiguity of a deep resistive region underlying a thick conductive layer is indeed intrinsic of the TDEM measurement and results from the modeling of EM induction in the Earth. It is independent of the adopted inversion approach and can be properly assessed only using another geophysical technique (e.g. resistivity tomography or magnetotelluric).

Generally, both SCI and 1D inversions tend to give higher resistivity values in the deepest portions of the models with respect to PSO. Due to the increased number of layers, the PSO results depict a

smoother transition between the shallow resistive portion of the model and the underlying low resistivity region. Within the low resistivity region, local high resistivity layers are also evident from the PSO results, but the reduced intrinsic resolution of the TDEM methodology at these depths cannot evidence such alternations. For site A5 the best fitting PSO inversion (Figure 5f) reports very low resistivity values from about 220 m to higher depth. This result is anomalous with respect to other PSO trials (grey dashed lines), and can be considered an indication of the reduced sensitivity of the optimization at great depths. Another explanation could be that the model with the minimum misfit (black line) led to a deep conductive artifact below the conductive layers due to a scarce influence of the regularization term of the PSO modeling. This outcome clearly shows the dramatic non-uniqueness of the inverse solution.

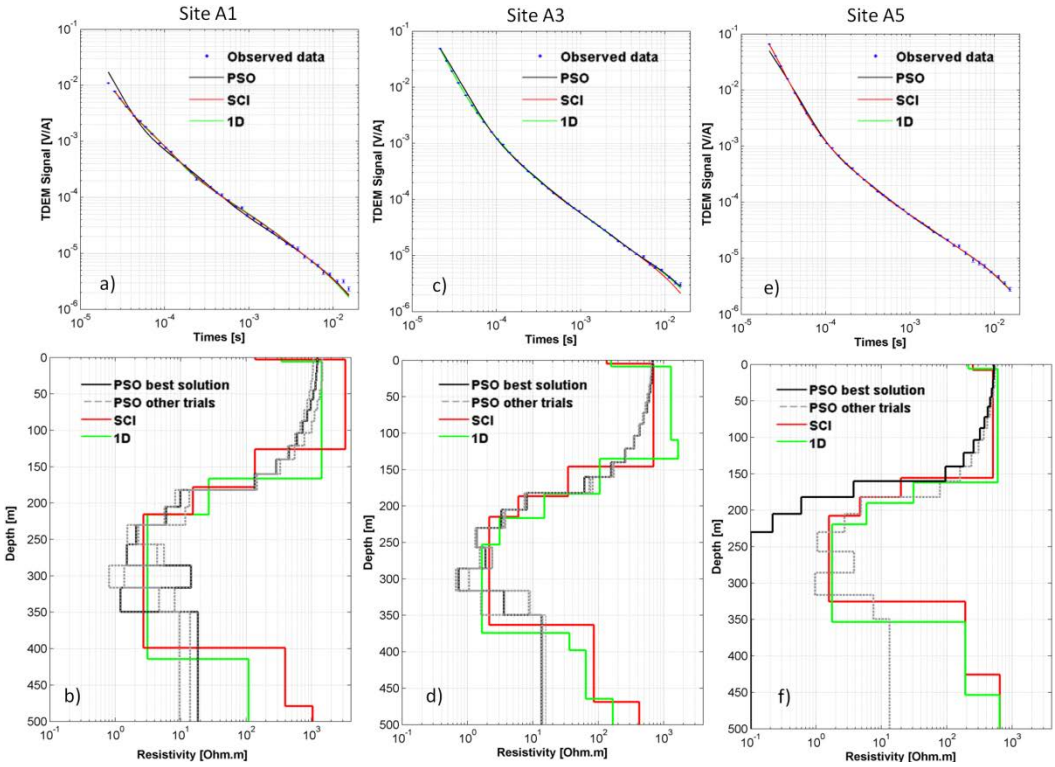

Figure 5 – Example results of the acquired data and of the different inversions for the soundings within the vineyard: a), c) and e) acquired TDEM data (blue dots) and simulated responses from PSO (black line), 1D inversion (green line) and SCI (red line); b), d) and f) inverted resistivity profiles resulted from the different inversion approaches: PSO best solution (black line), PSO other solutions (grey dashed line), 1D inversion (green line) and SCI (red line).

The lateral continuity of the geological setting below the vineyard can be better visualized with the pseudo-2D representation of the SCI inversion (Figure 6). With this visualization, it is possible to observe that the presence of a low resistivity region is depicted by almost all the soundings. Only in site A12 this low resistivity zone shows a reduced thickness (Figure 6).

In Figure 7, the results of the acquired data and of the different inversions for the soundings outside the vineyard are reported. For these soundings, SCI was not applied due to the poor spatial coverage. It can be observed that these results are different from those within the vineyard in terms of both the shape of the acquired TDEM signals and the inversion results. For these soundings, relatively more noisy data were acquired (see Figure 7c at late times) probably due to the proximity of electric disturbances (cables, pipelines) and the greater urbanization along the coastline. Nevertheless, the data fitting of the TDEM signals, despite higher than the soundings within the vineyard, can be considered satisfactory (on average below 5%) in all the sites (Figure 7a, c and e).

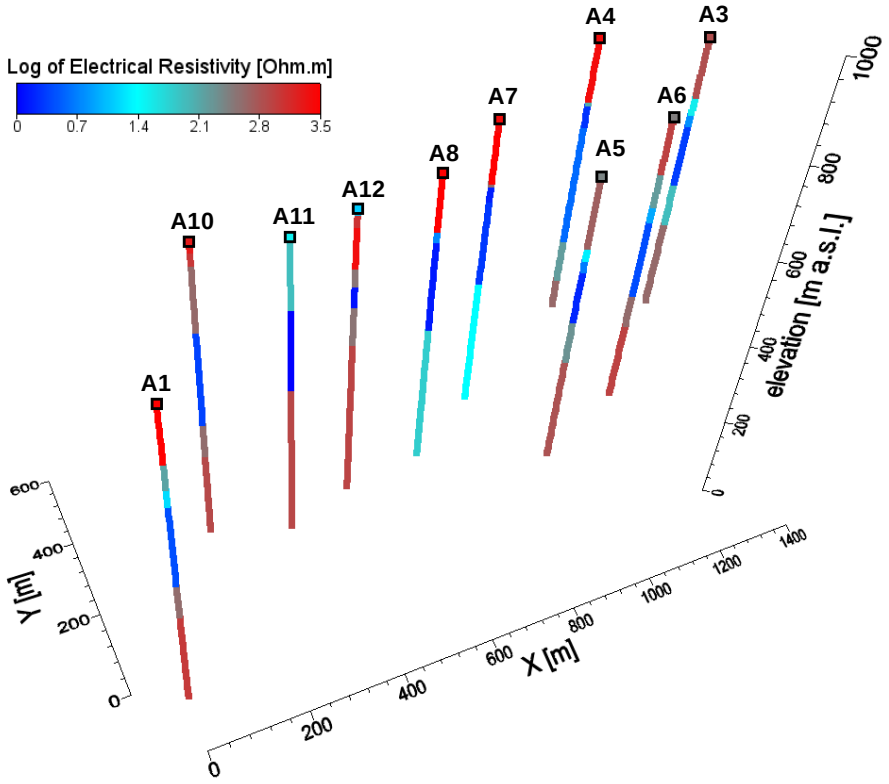

Figure 6 – Results of the SCI of the soundings within the vineyard: pseudo-2D view of the inverted resistivity profiles. Distances among the soundings (X and Y) are relative to A1 coordinates for greater clarity; real coordinates are reported in Table 1.

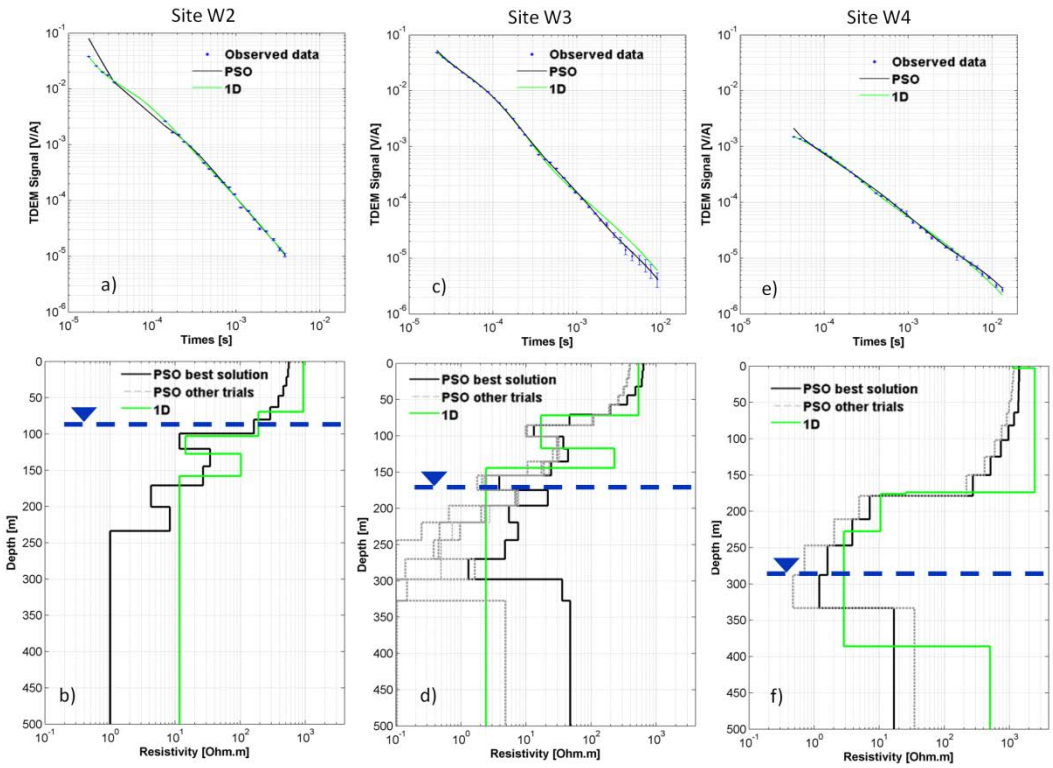

Figure 7 – Results of the acquired data and of the different inversions for the soundings outside the vineyard a), c) and e) acquired TDEM data (blue dots) and simulated responses from PSO (black line) and 1D inversion (green line); b), d) and f) inverted resistivity profiles resulted from the different inversion approaches: PSO best solution (black line), PSO other solutions (grey dashed line) and 1D inversion (green line). The sea level depth is also reported (blue dashed line).

The interpreted resistivity profiles (Figure 7b, d and f) depict the presence of a shallow high resistivity portion overlying a low resistivity region, relatively continuous at depth. With respect to the results within the vineyard (Figure 5) this low resistivity region appears shallower (at around 80 – 120 m b.g.l.) and with relatively higher resistivity values (around 50 Ωm). Sites W2 and W3 also report a resistivity drop (<10 Ωm) almost in correspondence of the sea level, while site W4 images a thick conductive region far before the sea interface.

5. DISCUSSION

All the different inversions performed showed consistent but partially different resistivity profiles, all with satisfactory data misfit. From the data misfit point of view, all the results can therefore be considered equivalent and only geological considerations could allow to select the most consistent ones with respect to a priori information and hydrogeological knowledge. The knowledge of stratigraphy and water table depths can indeed be important in the interpretation of TDEM soundings (Christiansen et al., 2006). Therefore, the association of depicted resistivity values to water-bearing formations and/or geological variability was attempted in relation to local stratigraphic information. Unfortunately, the available a priori information with this respect was very scarce in the Fogo Island context. Moreover, some of the provided information showed reduced reliability particularly concerning the water levels within the wells, since they may refer to different time ranges with respect to the performed surveys. Therefore, the considerations performed in the following have to be considered partially speculative.

In volcanic contexts in general, the potential presence of weathered tuff, one of the most common pyroclastic rocks, can be associated with a consistent drop in resistivity due to its contrast with more compact basaltic formations. Celico (1988) reports resistivity values ranging from 10 to 100 Ωm in tuff rocks, heavily depending on water saturation. Ruiz-Aguilar et al. (2010) measured 15 to 40 Ωm in an aquifer layer contained in tuff rocks from pyroclastic flows, in a TDEM survey in Mexico. In the same study, further drops in resistivity (1-5 Ωm) were related to clayish material. Gonçalves et al. (2017) performed a great number of TDEM profiles in Santiago Island on coastal sites with available stratigraphic information. Resistivities of about 10 Ωm corresponded to fresh groundwater hosted in various weathered layers, such as pyroclastic rocks, basalts, and coarse scoria. Lower resistivity values (1 Ωm) delineated the saltwater intrusion. These previous TDEM surveys reported values of resistivity associated with stratigraphic information about fresh aquifers, clayish material, saltwater aquifers, which are all elements potentially present in the Fogo setting. They can be therefore a first attempt benchmark for our TDEM survey, as long as the geologic and topographic differences are taken into proper account. The available geological and hydrogeological information of Fogo Island itself is related to a few wells located near our TDEM surveys outside the vineyard (W2, W3 and W4).

With this respect, in Figures 8 and 9 the results of surveys W2 and W3 are compared with the evidence of water table depth in the nearby wells. The presented results are focused on the evidence of TDEM soundings in correspondence with the water-table and the underlying seawater level. The resistivity distribution imaged at greater depths is less constrained as can be evidenced by the higher variations in the results of the different inversion strategies (Figure 7b and d). Unfortunately, no geologic

information on these wells is available and also the water table depth information can be partially critical due to the different time range in which it was acquired with respect to the present surveys.

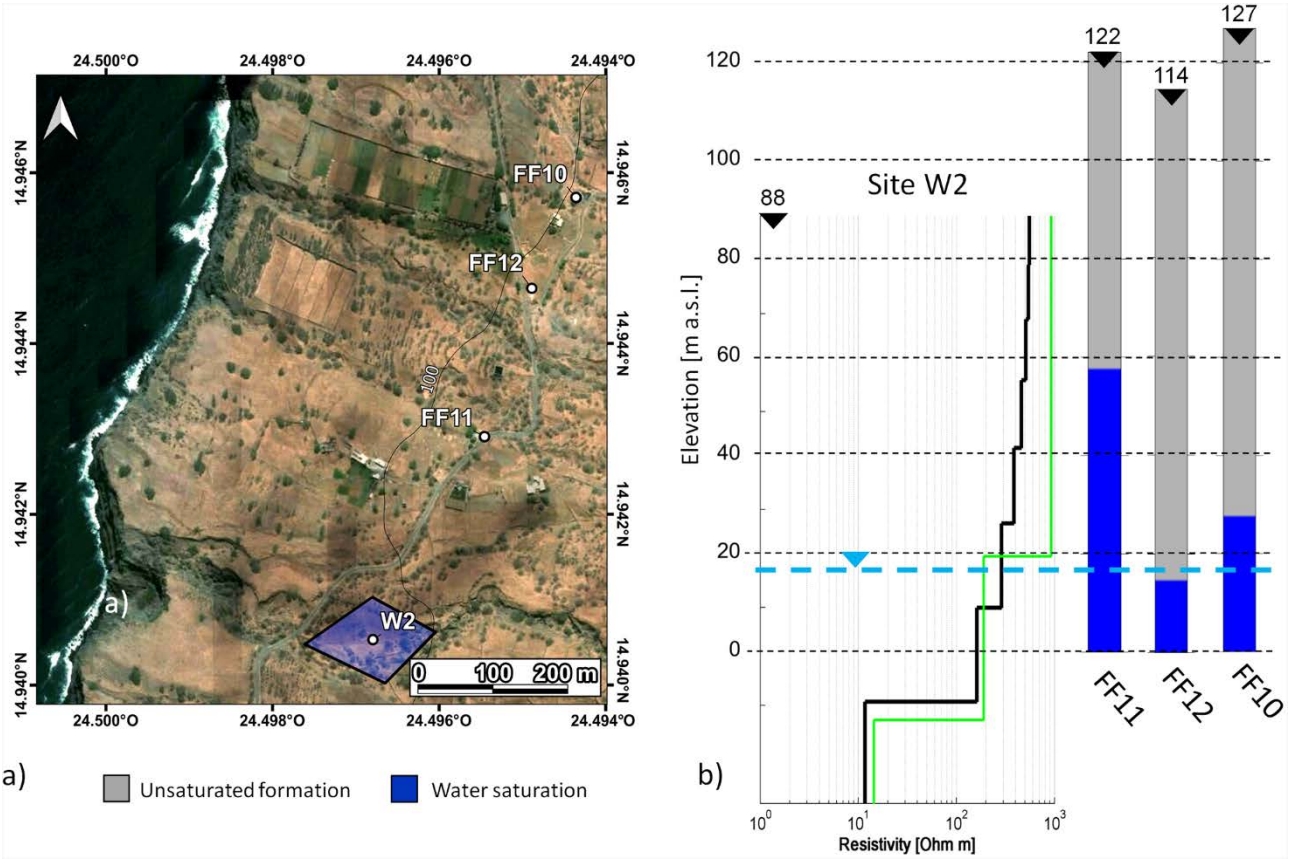

Figure 8– Results of survey W2 compared with the evidence of water table depth in three nearby wells: a) survey and water wells location, b) resistivity profile and the supposed water table depth compared to that of the wells.

From the W2 comparison (Figure 8), it can be evidenced that the 1D inversion, given its reduced layer parameterization, is more able than PSO to evidence the sharp transition in the stratigraphy related to the probable presence of water. The PSO inversion remains however an important step to be performed in order to avoid the result to be related to a local minimum. This transition can be located with the 1D result at the passage between the high-resistivity (about 900 Ωm) first layer and the lower-resistivity (about 200 Ωm) second layer. The resistivity drop can be attributed to water saturation. The presence of water at this depth is also evidenced by the data from FF12 well, given the fact that both the survey W2 and the FF12 well are located in morphological depressions. Greater discrepancies can conversely be observed with the FF11 and FF10 wells. Particularly, FF11 well, which is the nearest to our surveys, reports a significantly shallower water depth. This depth variability among the wells suggests a complicated water table distribution probably influenced by the fracture distribution within the rock and the potential presence of perched water lenses.

A further decrease in resistivity is also evidenced in the W2 survey below sea level. With this respect, both PSO and 1D results compare well in evidencing the lower resistivity (about 10 Ωm) of this deep

layer. If this layer is attributed to a seawater saturated formation, its resistivity value appears to be higher than that reported by Gonçalves et al. (2017) on Santiago island (i.e. 1 Ωm). This difference can be at first attempt attributed to possible differences in the rock matrix (i.e. porosity and/or fracture distribution) or in a partial seawater/freshwater mixing in the inland (i.e., presence of a brackish water layer).

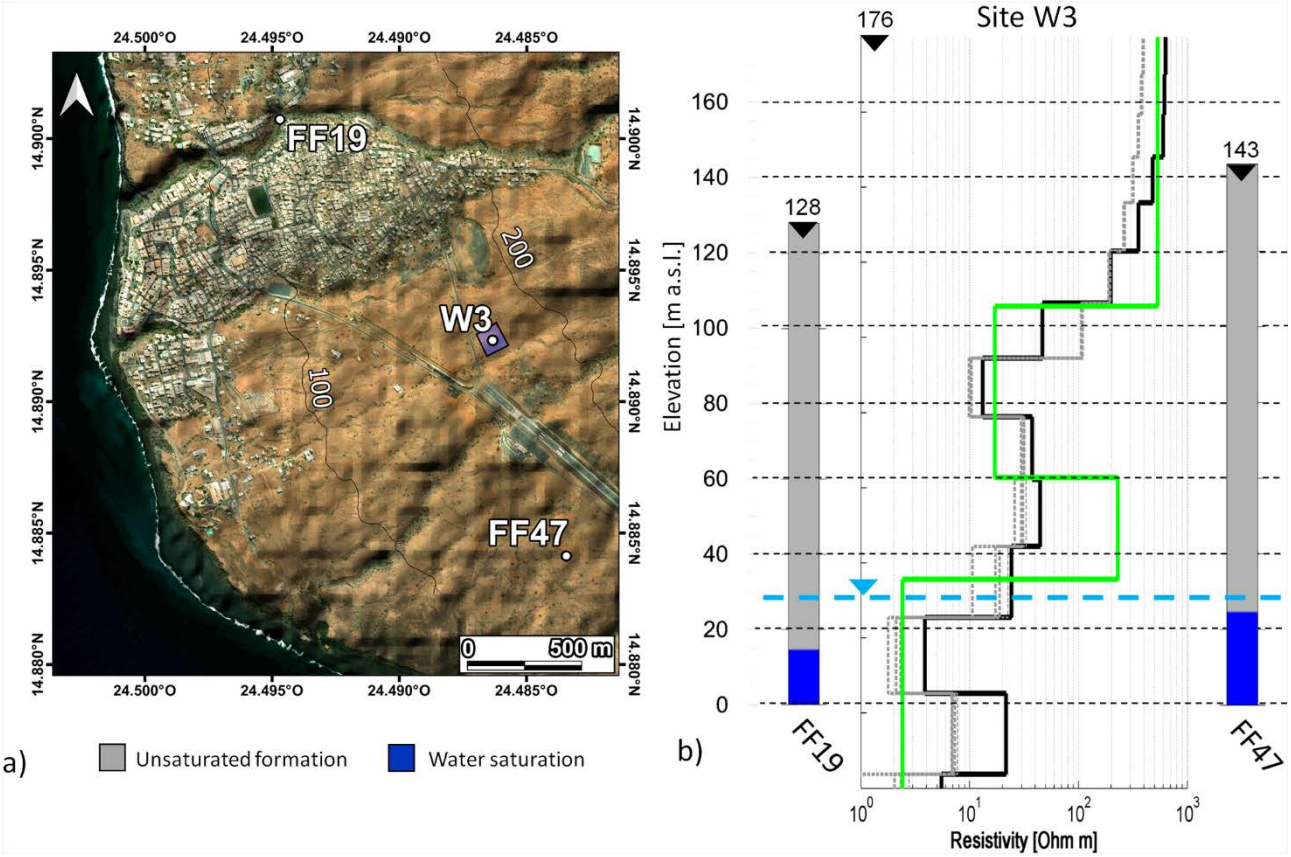

Figure 9– Results of survey W3 compared with the evidence of water table depth in two nearby wells: a) survey and water wells location, b) resistivity profile and water table depths.

The W3 survey (Figure 9), associates the water table layer with resistivity values much lower than W2 (about 5 Ωm). The depth of this resistivity drop in the TDEM profile compares well with the water table depth in two nearby wells. These different electrical resistivity values attributed to the water-saturated formation can be explained either by a different water electrolytic conductivity or a change in the lithology of the formation.

In order to discuss the difference between the W2 and W3 resistivity models, the information from nearby wells, in terms of water electrical conductivity, was considered. The average water conductivity of wells FF10-FF12 (near survey W2) is around 370 µS/cm while that of FF19-FF47 (near survey W3) is around 850 µS/cm. The increased water conductivity in wells FF19 and FF47 could be related to a more relevant seawater intrusion due to higher exploitation. The latter wells are indeed located near a highly urbanized area (see Figure 9a) and are subjected to increased water

demand. The higher water conductivity may reflect a lower resistivity for the water-saturated formation. However, the observed lower resistivity of the water-bearing formation could also be related to the presence of pyroclastic rocks (i.e. tuffs) which generally (see the above-mentioned literature references) show comparable resistivity ranges in saturated conditions or to the presence of weathered lavas or more clayish material..

As stated before, it was not possible to find reliable and detailed geologic information in these locations, therefore we attempt an indirect way to ascertain the nature of the observed differences between W2 and W3 in the resistivity values of the water-saturated formation. Computations with the use of Archie's law (Archie, 1942) as a function of the interstitial water conductivity are proposed in Table 2. For these computations, a constant formation porosity (i.e., 0.26) was assumed matching the observations of the W2 survey with standard Archie's parameters values (i.e., a=1 and m=1.5).

Table 2 – Application of Archie's law for different water conductivities of the interstitial fluid.

	Water Conductivity [μS/cm]	**Formation Resistivity [Ωm]**
freshwater FF10-FF12 wells	370	200
freshwater FF19 -FF47 wells	850	87
brackish water	7500	10
seawater	60000	1

From the results reported in Table 2, it can be observed that the resistivity value detected by the W2 survey (i.e. 200 Ωm), at the depth of the water table of the near FF10 and FF12 wells, is compatible with the water electrical conductivity measured in the wells (370 μS/cm), according to Archie's law. Instead, this is not true for the resistivity value detected by the W3 survey (i.e. around 5 Ωm), at the depth where the near wells extract water with a conductivity of 850 μS/cm. The only change in the water conductivity among the wells is therefore not able to explain alone the different resistivities (200 and 5 Ωm) observed in the W2 and W3 surveys in the aquifer layer.

It can also be noted in Table 2 that, according to Archie's law, only a saltwater intrusion can explain the values of around 10 and 1 Ωm, which match respectively the presence of brackish water in the

formation, as interpreted for the third layer of the W2 survey, and of seawater, as reported by Gonçalves et al. (2017) in a similar geological setting. However, the conductivity of 850 μS/cm of nearby wells does not suggest the presence of saltwater or brackish water in the W3 area at the water table level. If saltwater or brackish water are not present in the formation, the observed resistivity values in the same range can be attributed to the presence of a relevant surface conduction component (not considered in Archie's formulation) related to the rock solid skeleton. This therefore suggests that the observed resistivity values in the 1 to 10 Ωm range can be associated to the presence of clays promoting the hypothesis of perched aquifers, as probably is the case of the W3 well, and as also found by Gonçalves et al. (2017) in Santiago Island. In profile W3, a shallow resistivity drop is also evidenced around 100 m a.s.l.; this drop is then followed by an increase in resistivity, more marked in the 1D result. This resistivity behavior may be attributed either to the presence of suspended partially saturated formations or to potential pyroclastic levels.

Also for the W4 survey, a partial comparison can be attempted with available hydrogeological information. Notwithstanding the significant distance between the TDEM sounding and the FF40 well (see Figure 3a), useful considerations can be deduced from this comparison. First, it can be observed that the thin pyroclastic levels (Figure 2b) are not particularly evidenced from the survey results (Figure 7f) evidencing an almost constant resistivity value (around 2500 Ωm) till about 200 m b.g.l. depth. This is in line with the expected vertical resolution of the methodology and with the reduced resistivity difference between the basaltic and pyroclastic formations under unsaturated conditions. The known water-table depth below FF40 (see Figure 2b) lies at around 50 m a.s.l. and can be roughly associated with the low-resistivity region (around 10 Ωm) at around 200 m b.g.l. for site W4 (Figure 7f). Given the significant distance between the TDEM survey and the well also in this location, an acceptable comparison in the water table identification is therefore evidenced.

From the above-performed comparisons and computations by means of Archie's law, it can be deduced that water-saturated formations can be associated with resistivities ranging from around 200 Ωm , for freshwater-saturated formations, to around 10 Ωm, for brackish water-saturated formations, from our results, and to around 1 Ωm for seawater formations, from literature reference values. Lower resistivity values for freshwater-saturated formations, in the 1 – 10 Ωm range, can also be related to the presence of weathered lava or more clayish material. Conversely, unsaturated formations report significantly higher resistivity values (i.e. above 900 Ωm) thus allowing a clear distinction.

Within these resistivity ranges, the results obtained within the vineyard, where no direct information is available, can be tentatively interpreted to identify possible water-rich areas. In Figure 10 a pseudo-2D WE cross-section of the SCI inverted profiles executed in the vineyard is reported with a superimposed delineation of the main resistivity transitions. The subsurface of the vineyard can be

characterized by a shallow high-resistivity layer (around 1000 Ωm) from 100 to 200 m thick, associated with unsaturated basalt and pyroclastic rock, followed by a layer with a significant resistivity drop (1-10 Ωm) around 150 m thick, potentially associated with a water-saturated formation. The deepest layers of the models, even if at the limit of the investigation depth, report on a resistivity rise, which may be related to the bedrock. In Figure 10 a comparison is also made with the water-table depth interpreted by the Martínez-Moreno et al. (2016) surveys, without borehole evidence.

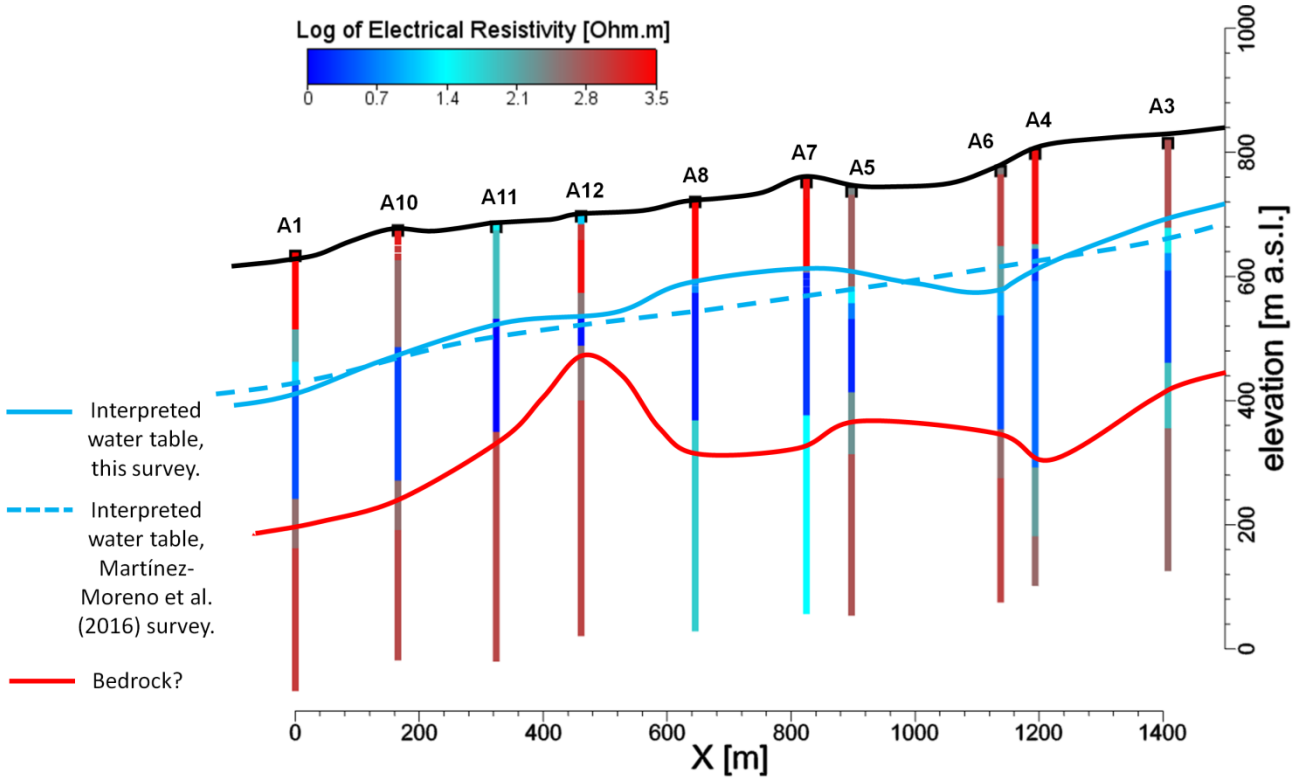

Figure 10 – WE cross-section of the profiles executed in the vineyard with a superimposed geological interpretation of the evidenced resistivity ranges. Distances among the soundings (X) are relative to A1 coordinates for greater clarity; real coordinates are reported in Table 1.

It can be observed that, notwithstanding the wider scale of the Martínez-Moreno et al. (2016) survey, with only one TDEM loop located near the vineyard, the water table interpreted by the two studies compares well. Differently from the Martínez-Moreno et al. (2016) interpretation, the present survey suggests the presence of a highly resistive formation at a certain depth below the sites. This evidence is near to the investigation limit for the surveys so it must be considered with caution. Nevertheless, the morphology of the evidenced formation may suggest the presence of a probable dyke along the profile, influencing the water-table shape. The presence of the dykes results indeed in barrier-like alterations of groundwater flow (e.g., Comte et al., 2017). Similar dykes are often frequent in volcanic environments due to the presence of secondary eruptive cones, which are clearly visible in different

locations along the west side of the island. Due to the distribution of the surveys along a pseudo-2D profile, it is not possible to discriminate if the evidenced dyke could be radial or circular.

This high-resistivity formation could act as an aquiclude for the surface water and configure the water-saturated layer as a suspended aquifer. This interpretation is solely based on geophysical evidence but is in our opinion more reliable than that of Martínez-Moreno et al. (2016) which conversely speculated the continuity of the water table till the contact with seawater for very relevant thicknesses (i.e. about 500 m). The evidenced resistivity ranges for the water-bearing formation (1-10 Ωm) are quite low, resembling the values seen in the survey W3. They can be explained, following the computations by means of Archie's law, with the presence of a weathered lava formation or more clayish material. This would configure the evidenced aquifer as a perched aquifer similar to what is observed near the coastline in some locations, in which probable clay lenses acted as aquiclude. Even under this second hypothesis, the presence of a certain amount of water within the formation is strongly suggested by the reduced resistivity values of this layer reported by the surveys, which are significantly different from the ones attributable to unsaturated formations.

Given the uncertainty of this interpretation in relation to the absence of a priori information near the vineyard, confirmation of the suggested geological setting is nevertheless required by the execution of further TDEM surveys nearer to known wells, the eventual use of different geophysical techniques (e.g. resistivity tomography) and the execution of explorative boreholes. The execution of a TDEM loop, for example near FF11 well, even if not logistically easy, could give more indication on the presence of perched aquifers in the inland. The execution of resistivity tomography surveys in the Fogo Island context would conversely be quite challenging and costly, given the need for several kilometers of multi-electrode cables, to reach resistive formations below conductive ones at more than 100 m depths. Alternative acquisition strategies (e.g., Troiano et al., 2019) could be eventually investigated involving the use of independent separations between sources and receiver voltage dipoles.

These further surveys could eventually increase the knowledge on the general geological setting, but most probably the crucial question marks, concerning the nature and continuity of the water formation within the vineyard, would remain not completely resolved till explorative drilling would be executed.

6. CONCLUSION

We investigated a vineyard planted in 2009 and recently affected by water scarcity, which has compromised its wine production. A pseudo-2D profile of TDEM soundings was created within the vineyard to detect potential drilling points for water wells. Further TDEM soundings were acquired outside the vineyard and along the coastline close to boreholes for which water depth information was available. The TDEM signal was interpreted following three different methods to assess the uncertainty of the results: the global-search algorithm (PSO), 1D linearized inversion with few-layers parametrization and spatially-constrained inversion (this only applied to the surveys in the vineyard). The choice of multiple interpretation methods represented a novelty with respect to the previous TDEM survey on the island (Martínez-Moreno et al., 2016) and had the advantage of comparing the different equivalent solutions of the TDEM inverse problem. Moreover, thanks to the tight spatial covering of the soundings in the vineyard, SCI was suitable and provided a detailed resistivity distribution of the subsurface in a pseudo-2D profile. This level of accuracy extended the large-scale resistivity model of Martínez-Moreno et al. (2016) and resulted in a more detailed geological interpretation in the vineyard.

Our results show that the subsurface of the vineyard is characterized by a shallow high-resistivity layer (around 1000 Ωm) from 100 to 200 m of thickness associated with unsaturated basalt and pyroclastic rock. This layer is followed by a layer with a significant resistivity drop (1-10 Ωm) whose thickness is around 150 m, except for a minimum in correspondence of a probable dyke. The deepest layers of the models, even if at the limit of investigation depth, imaged a resistivity rise, which may be related to the bedrock.

The main contribution of this work is to provide further knowledge on the electrical resistivity distribution in the subsurface of the vineyard and other isolated areas of the Island of Fogo. The results of the TDEM soundings far from the vineyard and the information from wells allowed to attempt correlations between the resistivity distribution and its hydrogeological interpretation. We suggest that the resistivity drop in the profiles can be attributed to water-saturated weathered lava formation or more clayish materials. A minor drawback of our investigation was the perturbed TDEM signal due to capacitive effects (the iron pickets inside the vineyard) and inductive effects. We managed this issue by repeating the acquisition for increasing time ranges.

We are confident that this work may be helpful for future wise exploitation of water resources on the island of Fogo. Further investigations should consider other geophysical exploration techniques, such as the self-potential or electric resistivity tomography methods, in order to more precisely confirm the interface of the water-table depth on the west side of the island of Fogo.

ACKNOWLEDGMENTS

This work was funded by AMSES (Associazione Missionaria Solidarietà e Sviluppo) Italian non-profit organisation of social utility which financed the survey campaign and travel costs for the authors. The authors are indebted to: Donika Sulejmani for her collaboration with the field data acquisition, Diego Franco for his help in preparing the instrumentation before the survey campaign and Prof. Alberto Godio for his precious advice to both fieldwork setting and processing.

REFERENCES

Archie, G.E., 1942. The Electrical Resistivity Log as an Aid in Determining Some Reservoir Characteristics. Transactions of the AIME 146, 54–62. https://doi.org/10.2118/942054-G

Auken, E., Violette, S., d'Ozouville, N., Deffontaines, B., Sørensen, K.I., Viezzoli, A., de Marsily, G., 2009. An integrated study of the hydrogeology of volcanic islands using helicopter borne transient electromagnetic: Application in the Galápagos Archipelago. Comptes Rendus Geoscience 341, 899–907. https://doi.org/10.1016/j.crte.2009.07.006

Barbosa, I.V.F., 2008. Gestão Integrada dos Recursos Hídricos na Ilha do Fogo (bachelor Thesis). Instituto superior de Educação, Praia, Cabo Verde.

Bear, J., Cheng, A.H.-D., Sorek, S., Ouazar, D., Herrera, I., 2010. Seawater Intrusion in Coastal Aquifers Concepts, Methods and Practices. Springer Netherlands, Dordrecht.

Celico, P., 1988. Prospezioni idrogeologiche. Liguori editore, Napoli.

Christiansen, A.V., Auken, E., Sørensen, K., 2006. The transient electromagnetic method, in: Kirsch, R. (Ed.), Groundwater Geophysics. Springer-Verlag, Berlin/Heidelberg, pp. 179–225. https://doi.org/10.1007/3-540-29387-6_6

Comina, C., Socco, L.V., Manzella, A., 2012. Pseudo-3D Characterization of a Geothermal Field through Magneto Telluric. Presented at the Near Surface Geoscience 2012 – 18th European Meeting of Environmental and Engineering Geophysics, Paris, France. https://doi.org/10.3997/2214-4609.20143382

Comte, J.-C., Wilson, C., Ofterdinger, U., González-Quirós, A., 2017. Effect of volcanic dykes on coastal groundwater flow and saltwater intrusion: A field-scale multiphysics approach and parameter evaluation: VOLCANIC DYKES AND GROUNDWATER FLOW. Water Resour. Res. 53, 2171–2198. https://doi.org/10.1002/2016WR019480

Danielsen, J.E., Auken, E., Jørgensen, F., Søndergaard, V., Sørensen, K.I., 2003. The application of the transient electromagnetic method in hydrogeophysical surveys. Journal of Applied Geophysics 53, 181–198. https://doi.org/10.1016/j.jappgeo.2003.08.004

Day, S.J., Heleno da Silva, S.I.N., Fonseca, J.F.B.D., 1999. A past giant lateral collapse and present-day flank instability of Fogo, Cape Verde Islands. Journal of Volcanology and Geothermal Research 94, 191–218. https://doi.org/10.1016/S0377-0273(99)00103-1

De Luca, D.A., Comina, C., Lasagna, M., Destefanis, E., Masciocco, L., Godio, A., Stocco, S., 2018. Effectiveness of geophysical surveys for water wells relocation in overexploited aquifers (the example of Maggiore and Traversola Valleys, Northwestern Italy). Environ Earth Sci 77, 19. https://doi.org/10.1007/s12665-017-7218-0

Descloitres, M., Guérin, R., Albouy, Y., Tabbagh, A., Ritz, M., 2000. Improvement in TDEM sounding interpretation in presence of induced polarization. A case study in resistive rocks of the Fogo volcano, Cape Verde Islands. Journal of Applied Geophysics 45, 1–18. https://doi.org/10.1016/S0926-9851(00)00015-X

Everett, M.E., 2013. Near-Surface Applied Geophysics. Cambridge University Press, Cambridge. https://doi.org/10.1017/CBO9781139088435

Falkland, A., Custodio, E., 1991. Hydrology and water resources of small islands: a practical guide: a contribution to the International Hydrological Programme, IHP-III, Project 4.6, Studies and reports in hydrology. Unesco, Paris.

Freeze, R.A., Cherry, J.A., Cherry, J.A., 1979. Groundwater. Prentice-Hall.

Gingerich, S.B., Voss, C.I., 2005. Three-dimensional variable-density flow simulation of a coastal aquifer in southern Oahu, Hawaii, USA. Hydrogeol J 13, 436–450. https://doi.org/10.1007/s10040-004-0371-z

Godio, A., Santilano, A., 2018. On the optimization of electromagnetic geophysical data: Application of the PSO algorithm. Journal of Applied Geophysics 148, 163–174. https://doi.org/10.1016/j.jappgeo.2017.11.016

Gonçalves, R., Farzamian, M., Monteiro Santos, F.A., Represas, P., Mota Gomes, A., Lobo de Pina, A.F., Almeida, E.P., 2017. Application of Time-Domain Electromagnetic Method in Investigating Saltwater Intrusion of Santiago Island (Cape Verde). Pure Appl. Geophys. 174, 4171–4182. https://doi.org/10.1007/s00024-017-1642-7

Heilweil, V.M., Earle, J.D., Cederberg, J.R., Messer, M.M., Jorgensen, B.E., Verstraeten, I.M., 2005. Evaluation of Baseline Ground-Water Conditions in the Mosteiros, Ribeira Paul, and Ribeira Fajã Basins, Republic of Cape Verde, West Africa.

Ingeman-Nielsen, T., Baumgartner, F., 2006. Numerical modelling of complex resistivity effects on a homogenous half-space at low frequencies. Geophys Prospect 54, 261–271. https://doi.org/10.1111/j.1365-2478.2006.00532.x

Kennedy, J., Eberhart, R., 1995. Particle swarm optimization, in: Proceedings of ICNN'95 - International Conference on Neural Networks. Presented at the ICNN'95 - International Conference on Neural Networks, IEEE, Perth, WA, Australia, pp. 1942–1948. https://doi.org/10.1109/ICNN.1995.488968

Machado, F., De Assunção, C.F.T., 1965. Carta geológica de Cabo Verde (na escala de 1/100,000): notícia explicativa da folha da ilha do Fogo-estudos petrográficos. 13, 4, 597-604. Ed. García de Orta. Lisboa.

Martínez-Moreno, F.J., Monteiro Santos, F.A., Madeira, J., Pous, J., Bernardo, I., Soares, A., Esteves, M., Adão, F., Ribeiro, J., Mata, J., Brum da Silveira, A., 2018. Investigating collapse structures in oceanic islands using magnetotelluric surveys: The case of Fogo Island in Cape Verde. Journal of Volcanology and Geothermal Research 357, 152–162. https://doi.org/10.1016/j.jvolgeores.2018.04.028

Martínez-Moreno, F.J., Monteiro-Santos, F.A., Madeira, J., Bernardo, I., Soares, A., Esteves, M., Adão, F., 2016. Water prospection in volcanic islands by Time Domain Electromagnetic (TDEM) surveying: The case study of the islands of Fogo and Santo Antão in Cape Verde. Journal of Applied Geophysics 134, 226–234. https://doi.org/10.1016/j.jappgeo.2016.09.020

Mitchell-Thomé, R.C., 1972. Outline of the geology of the Cape Verde Archipelago. Geol Rundsch 61, 1087–1109. https://doi.org/10.1007/BF01820907

Nabighian, M.N. (Ed.), 1991. Electromagnetic Methods in Applied Geophysics: Volume 2, Application, Parts A and B. Society of Exploration Geophysicists. https://doi.org/10.1190/1.9781560802686

Pace, F., Godio, A., Santilano, A., Comina, C., 2019a. Joint optimization of geophysical data using multi-objective swarm intelligence. Geophysical Journal International 218, 1502–1521. https://doi.org/10.1093/gji/ggz243

Pace, F., Santilano, A., Godio, A., 2019b. Particle swarm optimization of 2D magnetotelluric data. GEOPHYSICS 84, E125–E141. https://doi.org/10.1190/geo2018-0166.1

Ratnaweera, A., Halgamuge, S.K., Watson, H.C., 2004. Self-Organizing Hierarchical Particle Swarm Optimizer With Time-Varying Acceleration Coefficients. IEEE Trans. Evol. Computat. 8, 240–255. https://doi.org/10.1109/TEVC.2004.826071

Ruiz-Aguilar, D., Arango-Galván, C., Hernández-Espriú, J.A., Arias-Paz, A., 2010. Aquifer assessment in Alfajayucan (Hidalgo, México) using TDEM. Presented at the 20th IAGA WG Workshop on Electromagnetic Induction in the Earth, Giza, Egypt.

Santilano, A., Godio, A., Manzella, A., 2018. Particle swarm optimization for simultaneous analysis of magnetotelluric and time-domain electromagnetic data. GEOPHYSICS 83, E151–E159. https://doi.org/10.1190/geo2017-0261.1

Sen, M.K., Stoffa, P.L., 2013. Global Optimization Methods in Geophysical Inversion. Cambridge University Press, Cambridge. https://doi.org/10.1017/CBO9780511997570

Sørensen, K.I., Auken, E., Thomsen, P., 2000. Tdem In Groundwater Mapping - A Continuous Approach, in: 13th EEGS Symposium on the Application of Geophysics to Engineering and Environmental Problems. Presented at the 13th EEGS Symposium on the Application of Geophysics to Engineering and Environmental Problems, European Association of Geoscientists & Engineers, Arlington, Virginia, USA,. https://doi.org/10.3997/2214-4609-pdb.200.2000_057

Spichak, V.V., 2015. Electromagnetic sounding of the Earth's interior.

Tarantola, A., 2005. Inverse Problem Theory and Methods for Model Parameter Estimation. Society for Industrial and Applied Mathematics. https://doi.org/10.1137/1.9780898717921

Troiano, A., Isaia, R., Di Giuseppe, M.G., Tramparulo, F.D.A., Vitale, S., 2019. Deep Electrical Resistivity Tomography for a 3D picture of the most active sector of Campi Flegrei caldera. Sci Rep 9, 15124. https://doi.org/10.1038/s41598-019-51568-0

Trota, A., Martinez-Moreno, F.J., Monjardino, P., Santos, F.A.M., Bernardo, I., Raposo, P., Ekstrom, M., Goncalves, S., Cabral, J., 2019. Investigating Perched Aquifers in Volcanic Terrains using TDEM Geophysical Exploration Technique. Presented at the International Conference on Engineering Applications, ICEA.

Viezzoli, A., Christiansen, A.V., Auken, E., Sørensen, K., 2008. Quasi-3D modeling of airborne TEM data by spatially constrained inversion. GEOPHYSICS 73, F105–F113. https://doi.org/10.1190/1.2895521